Solar Energy Materials & Solar Cells 94 (2010) 578–582

Contents lists available at ScienceDirect

Solar Energy Materials & Solar Cells

journal homepage: www.elsevier.com/locate/solmat

Extraction of solar cell series resistance without presumed current–voltage functional form

Ming-Kun Lee [a], Jen-Chun Wang [a], Sheng-Fu Horng [a,*], Hsin-Fei Meng [b]

[a] Department of Electrical Engineering, National Tsing Hua University, Hsinchu 300, Taiwan, Republic of China
[b] Institute of Physics, National Chiao Tung University, Hsinchu 300, Taiwan, Republic of China

ARTICLE INFO

Article history:
Received 30 June 2009
Received in revised form
22 November 2009
Accepted 24 November 2009
Available online 29 December 2009

Keywords:
Solar cell
Circuit model
Series resistance extraction

ABSTRACT

A new method which does not require presumed current–voltage functional form is proposed for the determination of the series resistance, the shunt resistance, the photocurrent, and the intrinsic current–voltage characteristics of solar cells. This method was applied to analyze a bulk heterojunction organic solar cell. It was found that the extracted intrinsic current–voltage characteristic clearly exhibits a linear hopping current component and a quadratic space-charge limited current component. Furthermore, the reconstructed dark current–voltage curve is found to differ significantly from the measured dark current–voltage curve, revealing the importance of electric field in the operation of bulk heterojunction organic solar cells.

1. Introduction

Solar cells are promising devices for clean electric generation and have attracted intensive research. Like all other electrical power generators, solar cells possess internal series resistance which affects significantly their power conversion efficiency (PCE). Moreover, the simulation and design of solar cell systems also require an accurate knowledge of the series resistance and other related device parameters to describe their nonlinear electrical behavior. Extracting the series resistance as well as other device parameters for solar cells is therefore of vital importance.

Over the years, various methods have been proposed for extracting the series resistance and related device parameters of solar cells [1–13]. These methods either involve current–voltage (*I–V*) measurements with different illumination levels [1–3,8], or apply curve fitting method to some presumed functional relationship [5–7,9–12], or employ integration procedures based on the computation of the area under the *I–V* curves [4], or use linear regression [13].

However, all these previously proposed methods are based on the assumption that the intrinsic *I–V* relationship of the solar cell follows a specific functional form, which is usually taken to be one or combination of the Shockley-type single exponential *I–V* characteristic with ideality factor. While the exponential *I–V* assumption may produce convenient equivalent-circuit model for use in conventional simulation tools, its validity, and hence its usefulness in understanding the underlying physics, is generally not guaranteed. This is especially the case for non p–n junction type devices such as organic solar cell (OSC) or dye-sensitized solar cell. For example, one would expect polynomial type intrinsic *I–V* characteristics for OSC if the charge transport is dominantly space-charge-limited (SCL). It is therefore advantageous to be able to extract the series resistance and device parameters without presumed *I–V* functional form. Such a series resistance extraction method without presumed *I–V* functional form is proposed in this paper. We found that with certain physically plausible assumptions such a scheme will lead to unique determination of all the device parameters as well as the intrinsic *I–V* characteristics. This method was applied to OSC and first-order hopping current and second-order SCL current components were observed in the intrinsic *I–V* characteristics.

2. Theory

The solar cell is characterized using the equivalent circuit model as shown in Fig. 1 and the relation between the measured current I_m and the measured voltage V_m is given by

$$I_m = \frac{V_D}{R_{sh}} + f(V_D) - I_{ph} \tag{1}$$

$$V_m = V_D + \left[\frac{V_D}{R_{sh}} + f(V_D) - I_{ph}\right] \cdot R_s \tag{2}$$

where V_D, $f(V_D)$, I_{ph}, R_s and R_{sh}, are the voltage across the diode, the intrinsic *I–V* characteristics of the diode, the photocurrent, the

* Corresponding author. Tel.: +886 35915873.
E-mail address: sfhorng@itri.org.tw (S.-F. Horng).

0927-0248/$ - see front matter © 2009 Elsevier B.V. All rights reserved.
doi:10.1016/j.solmat.2009.11.026

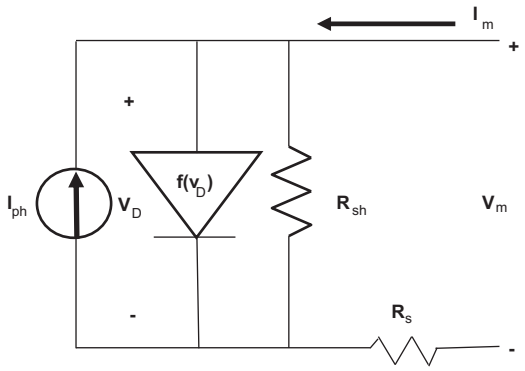

Fig. 1. The circuit model for solar cells.

series resistance and the shunt resistance, respectively. Note from Fig. 1 that since both $f(V_D)$ and R_{sh} are to be determined and are in parallel connection, any combination of $f(V_D)$ and R_{sh} that preserves the value $V_D/R_{sh}+f(V_D)$ will leave the measured I–V characteristics, I_m and V_m, unchanged. One therefore needs more assumptions to allow for unique determination of these device parameters. The following for assumptions are taken in our fitting scheme:

1. R_s, R_{sh}, I_{ph} remain constant during the measurements;
2. $f(0)=0$, that is, the power generation is all attributed to I_{ph};
3. $f(V_D)\rightarrow -f_0$ as $V_D \ll 0$; that is, the leakage current is attributed to R_{sh};
4. $f(V_D)$ is a monotonic function of V_D;
5. $f(V_D)$ is nonlinear for $V_D > 0$;
6. I_{ph} changes monotonically with illumination level.

From assumption 4 and (2), V_m is also a monotonic function of V_D, and $V_m \ll 0$ when $V_D \ll 0$. From assumption 3 for $V_m \ll 0$, one can eliminate V_D from both (1) and (2) and obtain

$$I_m = \frac{1}{(R_{sh}+R_s)}\cdot V_m - \frac{R_{sh}}{(R_{sh}+R_s)}\cdot (f_0+I_{ph}) \tag{3}$$

The total resistance $R_t = R_{sh}+R_s$ can therefore be obtained from the slope dI_m/dV_m at $V_m \ll 0$.

From (1) and (2) one can obtain

$$V_D = V_m - R_s\cdot I_m \tag{4}$$

$$f(V_D) = \frac{R_t}{(R_t-R_s)}\cdot I_m - \frac{V_m}{(R_t-R_s)} + I_{ph} \tag{5}$$

Considering also assumption 2, one also has

$$I_{ph} = -I_m(V_m @ V_D = 0) \tag{6}$$

It is clear from (3), (4) and (5) that since R_t can be extracted from the measured I–V characteristics, once R_s is determined, all other device parameters, namely R_{sh}, I_{ph} and the intrinsic I–V characteristics $f(V_D)$ can all be extracted. We now need a scheme to determine R_s.

In order to devise a scheme for the unique determination of R_s, we construct the following test quantities for arbitrary R:

$$V_{DR} = V_m - R\cdot I_m \tag{7}$$

$$I_{phR} = -I_m(V_m @ V_{DR} = 0) \tag{8}$$

$$f_R = \frac{R_t}{(R_t-R)}\cdot I_m - \frac{V_m}{(R_t-R)} + I_{phR} \tag{9}$$

Denote as V_{D0} the voltage across the diode when $V_{DR}=0$. It is clear that if $R=R_s$, then V_{DR}, f_R and I_{phR} reduce to V_D, f and I_{ph}, respectively, and $V_{D0}=0$.

For $R \neq R_s$, as derived in appendix, we have the following three equalities:

$$f(V_{D0}) = \frac{(R_t-R)}{R_{sh}\cdot(R-R_s)}\cdot V_{D0} + I_{ph} \tag{10}$$

$$f_R = \frac{R_{sh}}{(R_t-R)}\cdot (f(V_D)-f(V_{D0})) \tag{11}$$

$$f_R = \frac{R_{sh}}{(R_t-R)\cdot(R_s-R)}\cdot V_{DR} + \frac{1}{(R-R_s)}\cdot (V_D-V_{D0}) \tag{12}$$

It is obvious from (10) that V_{D0} depends on both I_{ph} and R.

For a given $f(V_D)$, one can expand it into Taylor series around V_{D0},

$$f(V_D) = f(V_{D0}) + f'(V_{D0})\cdot(V_D-V_{D0}) + \frac{1}{2!}f''(V_{D0})\cdot(V_D-V_{D0})^2 + \cdots \tag{13}$$

Combining (11)–(13), we have

$$\frac{R_{sh}}{(R_t-R)(R_s-R)}V_{DR} + \frac{1}{(R-R_s)}(V_D-V_{D0}) = \frac{R_{sh}}{(R_t-R)}\left[f'(V_{D0})(V_D-V_{D0}) + \frac{1}{2!}f''(V_{D0})(V_D-V_{D0})^2 + \cdots\right] \tag{14}$$

For a given $f(V_D)$, one can solve (V_D-V_{D0}) from (14) and substitute the result into (12) to obtain the functional relationship between f_R and V_{DR}. Since, from 5, $f(V_D)$ is nonlinear in V_D, the coefficients in the expansion (13) cannot be all constant and must depend on V_{D0}. Therefore, (V_D-V_{D0}) and hence f_R must also depend on V_{D0}.

From the aforementioned discussion, we know that unless $R=R_s$, at which V_{D0} vanishes identically, $f_R(V_{DR})$ must depend on V_{D0} and hence on I_{ph} and illumination level (6). At a specific R, we may therefore use the root-mean-square error (RMSE) between $f_R(V_{DR})$ at different illumination levels to determine if R coincides with R_s. Alternatively one may use the extracted $f_R(V_{DR})$ from the I–V measurement at one illumination level to reconstruct the measured I–V at another illumination and calculate the RMSE. It is noteworthy that to avoid the temperature difference due to different illumination levels, which might lead to significant extraction error [12,14], it is suggested that close illumination levels are used. In practice close illumination levels also ensure the constancy of R_s, R_{sh} required in assumption 1 and ascertain that identical R_t from both I–V characteristics can be obtained. Since R_s and R_{sh} are sensitive to cell temperature and illumination level, the constancy of R_t is an important indicator that assumption 1 is met. Note also that our extraction algorithm does not require the precise ratio in the illumination levels.

Our R_s extracting scheme is summarized as follows:

1. measure I–V characteristics $I_{m1}(V_m)$ and $I_{m2}(V_m)$ at two different illumination levels;
2. extract R_t from both $I_{m1}(V_m)$ and $I_{m2}(V_m)$ according to (3);
3. for a given R construct V_{DR1}, f_{R1} and I_{phR1} according to (7)–(9) from $I_{m1}(V_m)$;
4. extract I_{phR2} according to (7) and (8) from $I_{m2}(V_m)$;
5. reconstruct $I_{reconstruct2}(V_m)$ from V_{DR1}, f_{R1} and I_{phR2};
6. calculate the RMSE between $I_{m2}(V_m)$ and $I_{reconstruct2}(V_m)$;
7. repeat 3–5 for another R and search for minimum of RMSE.

Although too straightforward to be included in this paper, we have checked the validity of this fitting scheme (steps 3–7) with numerically generated data. It was found that the discrepancy in the fitting result was set by the error in the estimated R_t. It is therefore advisable to estimate R_t at sufficiently negative bias.

Since our R_s extracting scheme does not require specific I–V functional form, it can be applied to various kinds of solar cells as long as the assumptions are met. In particular it is interesting to apply this method to non p–n junction type photovoltaic devices to see if new insights may be obtained. In this paper a bulk heterojunction (BHJ) OSC was employed.

Organic photovoltaic devices have attracted much attention due to their promising properties such as mechanical flexibility, light weight and environmental benignity. In addition, because of their low-temperature and solution-based processability, they can be fabricated on flexible substrate, which can be adapted to high throughput continuous roll-to-roll manufacturing and leads to greatly reduced production cost. Due to strong Coulomb interaction in organic materials, photo-excited charged carriers quickly form excitons, with which charge separation by electric field typically used in p–n junction type solar cells is ineffective. Donor-acceptor type-II heterojunctions such as BHJ were demonstrated to be effective for exciton dissociation. With various structure, material and process advancements, the PCE of OSCs has been significantly improved and a record high PCE of 7.6% was recently reported [15]. All-solution roll-to-roll manufacturing processes for OSCs have also been designed and studied [16,17].

3. Experiment

In this study the BHJ OSC is made of a blend of poly (3-hexylthiophene) (P3HT) and 6,6-phenyl-C61-butyric acid methyl ester (PCBM) in a 1:1 weight ratio. The blend is sandwiched in between an indium tin oxide (ITO) coated-glass (sheet resistance $10\,\Omega/\square$)/poly(3,4 ethylenedioxythiophene): poly(styrenesulfonate) (PEDOT:PSS), and an evaporated calcium (50 nm)/silver (80 nm) top electrode. The thickness of the active layer is 220 nm and the area of the OSC is $4\,mm^2$. The fabrication procedure is standard and follows that in Ref. [18]. After fabrication the I–V characteristics was measured with a calibrated solar simulator at AM1.5G ($100\,mW/cm^2$). To obtain the I–V curve at a different light intensity, a microscope cover glass was placed on top of the OSC, leading to a light attenuation of about 8%. The RSME is calculated for the range from $V_D = 0$ to open-circuit voltage (Voc) in the measured I–V characteristic with less light illumination.

4. Results and discussion

Fig. 2 shows the measured $I_{m1}(V_m)$ and $I_{m2}(V_m)$ as well as dark I–V. The comparison of $I_{m2}(V_m)$ with the reconstructed I–V, as described in step 5, in the extraction scheme, is shown in Fig. 3, showing very good agreement between the measurement and the fitting curve. The fitting result is summarized in Table 1.

Fig. 4(a) and (b) show the extracted intrinsic device I–V characteristics in log–log and semi-log scale, respectively. A linear and a quadratic component can be clearly resolved in Fig. 4(a). The linear component is tentatively attributed to the hopping conduction, which dominates the carrier transport in disordered organic materials and can be linearized at low field [19]. The quadratic component is attributed to the SCL current transport frequently observed in organic materials. For comparison, the dark I–V, along with lines with the required slope, was also plotted in the insets of Fig. 4(a) and (b). It was found that the linear and quadratic current components can be resolved only after the removal of series and shunt resistance. It is also interesting to see from Fig. 4(b) that there is a 120 mV/dec exponential component in the extract intrinsic I–V, which may result from trap-assisted photo-carrier recombination. However,

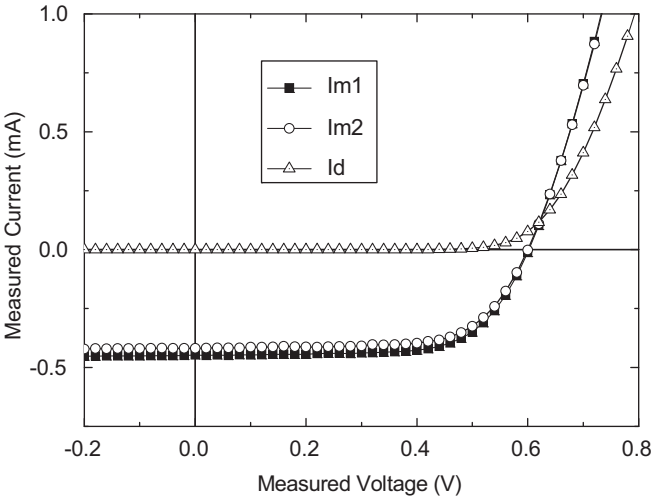

Fig. 2. Measured I–V characteristics at two illumination levels (I_{m1}, I_{m2}) and dark I–V (I_d) of the OSC.

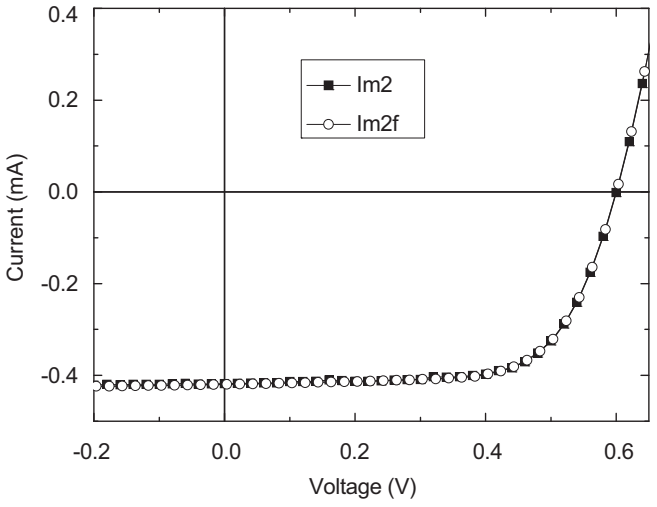

Fig. 3. The comparison of the measured illuminated I–V (I_{m2}) and the reconstructed I–V (I_{m2f}) as described in step 5 of the extraction scheme.

Table 1
The fitting parameters including R_s, R_{sh}, J_{ph1} and J_{ph2} for organic solar cell.

	R_s ($\Omega\,cm^2$)	R_{sh} ($\Omega\,cm^2$)	J_{ph1} (mA/cm^2)	J_{ph2} (mA/cm^2)
Organic solar cell	5.24	3060	11.3	10.5

the origin of this exponential component remains unclear and further investigation is required.

Fig. 5 shows the comparison of the measured and the reconstructed dark I–V characteristics. The latter was calculated as in step 5 yet with photocurrent set to zero. It was found that dramatic difference exists between these two I–V curves. It is well known that the dominant charge transport mechanisms in disordered organic materials are either hopping or SCL transport and depend strongly on the field distribution within the device. Since the carrier concentration, and therefore the field distribution, in the device changes significantly with light illumination, the reconstructed I–V characteristics from device parameters extracted from illuminated device will be different from the measured dark I–V. This result also corroborates the

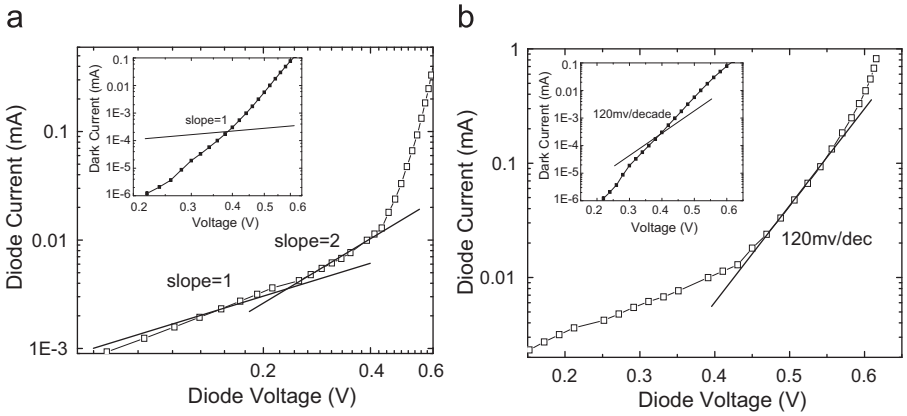

Fig. 4. The extracted intrinsic *I–V* in (a) log–log scale, showing clearly a linear and a quadratic current component; (b) in semi-log scale; note that an exponential component with a slope of 120 mV/dec was clear seen. The measured dark *I–V* was also plotted in the insets for comparison.

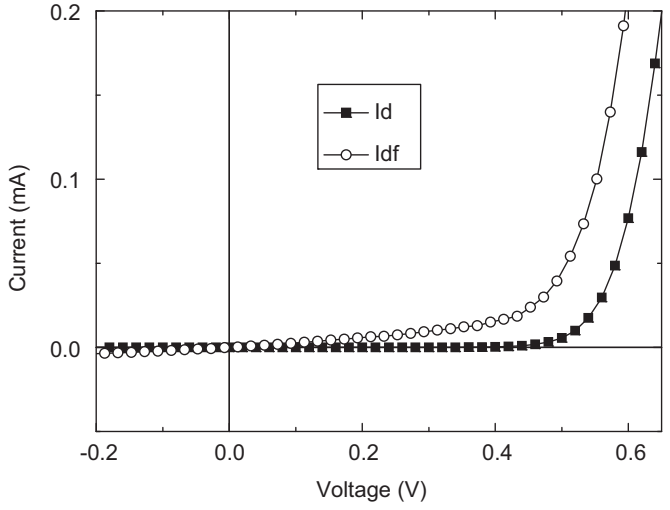

Fig. 5. The comparison of the measured dark *I–V* (I_d) and the reconstructed dark *I–V* (I_{df}) as described in step 5 of the extraction scheme, albeit with I_{ph} set to zero.

Table 2
The fitting parameters including R_s, R_{sh}, J_{ph1} and J_{ph2} for silicon solar cell.

	R_s (Ω cm^2)	R_{sh} (Ω cm^2)	J_{ph1} (mA/cm^2)	J_{ph2} (mA/cm^2)
Multi-crystal silicon	3.5	489	40.7	38.8
Amorphous silicon	14.7	2619	12.6	11.8

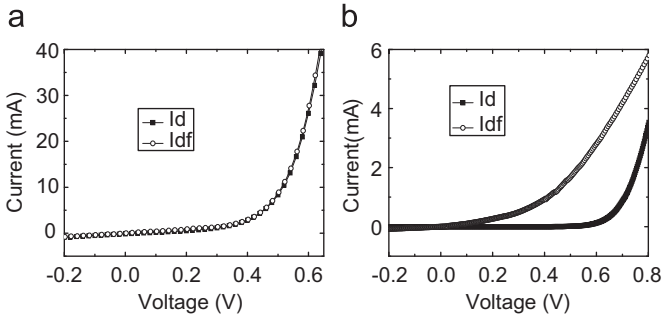

Fig. 6. The comparison of the measured dark *I–V* (I_d) and the reconstructed dark *I–V* (I_{df}) for (a) multi-crystal and (b) amorphous Si solar cell, respectively.

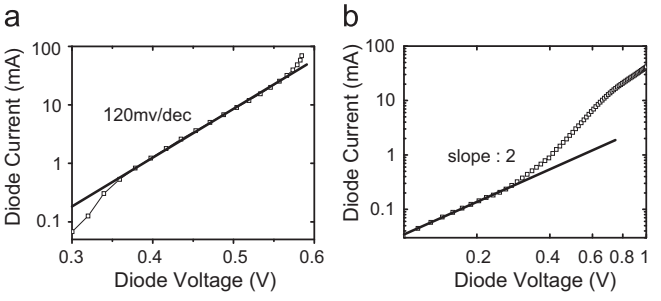

Fig. 7. The extracted intrinsic device *I–V* characteristics plotted in (a) semi-log scale for the multi-crystal and (b) log–log scale for amorphous Si solar cell, respectively.

needs for close illumination levels previously proposed in our extraction scheme.

For comparison we have also applied our R_s extraction scheme to a multi-crystal Si solar cell as well as an amorphous Si solar cell. These two solar cells were obtained from the Photovoltaics Technology Center at Industrial Technology Research Institute, Taiwan. The size for the multi-crystal (amorphous) Si solar cell is 2.13 (1.68) cm^2. The fitting results are summarized in Table 2. Fig. 6(a) and (b) show the comparison of the measured and the reconstructed dark *I–V* characteristics for multi-crystal and amorphous Si solar cell, respectively. From Fig. 6, it was found that, while very good agreement between the measured and the reconstructed dark *I–V* characteristics was obtained for the multi-crystal solar cell, there is dramatic difference in the case of amorphous Si solar cell. These results are not surprising since they simply reflect the difference between diffusion controlled carrier transport in bulk Si solar cell and drift current controlled, and hence electric field dependent, carrier transport in amorphous Si solar cell. Though disorder related traps in amorphous Si may also contribute additionally to the difference between the measured and the reconstructed dark *I–V* characteristics, these results are consistent with our previous argument of electric field effect on dark *I–V* in OSC.

Fig. 7(a) and (b) show the extracted intrinsic device *I–V* characteristics plotted in semi-log scale for the multi-crystal and log–log scale for amorphous Si solar cell, respectively. From Fig. 7(a) multi-crystal Si solar cell exhibits mostly single exponential *I–V* characteristic with ideality factor 2 as expected. On the other hand, it is clear from Fig. 7(b) that there is a quadratic current component at low voltage for amorphous Si

solar cell. This quadratic current component may also result from SCL transport; however, further investigation is required to clarify its nature.

5. Conclusion

In summary, a series resistance extraction scheme which requires no presumed *I–V* functional form was proposed. With *I–V* measurement at two illumination levels, all device-level parameters, including series resistance, shunt resistance, photocurrent and intrinsic *I–V* characteristics can be determined. This method was applied to analyze a BHJ OSC. We found that, after the removal of the series resistance, a linear hopping current component as well as a quadratic SCL current component can be clearly identified in the extracted intrinsic *I–V* characteristics. Furthermore, the reconstructed dark *I–V* is found to differ from the measured dark *I–V*, revealing the important role of electric field in BHJ OSC.

Acknowledgment

This work is supported by the National Science Council of Taiwan under Grant no. NSC97-2120-M-007-004 and NSC97-2628-M-009-016.

Appendix

Combine (1), (8) and (10), we get

$$I_{phR} = \frac{V_{D0}}{R_s - R} \tag{15}$$

Substitute (1), (2) into (7), we have

$$V_{DR} = \frac{(R_t - R)}{R_{sh}} \cdot V_D + (R_s - R) \cdot f(V_D) - (R_s - R) \cdot I_{ph} \tag{16}$$

Therefore, one gets

$$f(V_D) = \frac{V_{DR}}{(R_s - R)} - \frac{(R_t - R)}{R_{sh} \cdot (R_s - R)} \cdot V_D + I_{ph} \tag{17}$$

and

$$V_D = \frac{R_{sh}}{(R_t - R)} \cdot V_{DR} - \frac{R_{sh} \cdot (R_s - R)}{(R_t - R)} \cdot f(V_D) + \frac{R_{sh} \cdot (R_s - R)}{(R_t - R)} \cdot I_{ph} \tag{18}$$

Note also from (4) and (7)

$$I_m = \frac{V_{DR} - V_D}{R_s - R} \tag{19}$$

Solve V_m from (4) and substitute the result as well as (15), (18) and (19) into (9), we have

$$f_R = \frac{R_{sh}}{(R_t - R)} \cdot f(V_D) - \frac{R_{sh}}{(R_t - R)} \cdot I_{ph} + \frac{1}{(R_s - R)} \cdot V_{D0} \tag{20}$$

From (10)

$$I_{ph} = f(V_{D0}) - \frac{(R_t - R)}{R_{sh} \cdot (R - R_s)} \cdot V_{D0} \tag{21}$$

Substituting (21) into (20) leads to (11) and substituting (10) and (17) into (11) leads to (12).

References

[1] M. Wolf, H. Rauschenbach, Series resistance effects on solar cells measurements, Adv. Energy Convers. 3 (1963) 455–479.
[2] R.J. Handy, Theoretical analysis of the series resistance of a solar cell, Solid-State Electron. 10 (1967) 765–775.
[3] K. Rajkanan, J. Shewchun, A better approach to the evaluation of the series resistance of solar cells, Solid-State Electron. 22 (1979) 193–197.
[4] G.L. Araujo, E. Sanchez, A new method for experimental determination of the series resistance of a solar cell, IEEE Trans. Electron. Dev. 29 (1982) 1511–1513.
[5] T. Easwarakhanthan, J. Bottin, I. Bouhouch, C. Boutrit, Nonlinear minimization algorithm for determining the solar cell parameters with microcomputers, Int. J. Sol. Energy 4 (1986) 1–12.
[6] M. Chegaar, Z. Ouennouchi, A. Hoffmann, A new method for evaluating illuminated solar cell parameters, Solid-State Electron. 45 (2001) 293–296.
[7] A. Kaminski, J.J. Marchand, A. Laugier, *I–V* methods to extract junction parameters with special emphasis on low series resistance, Solid-State Electron. 43 (1999) 741–745.
[8] E. Radziemska, Dark I-U-T measurements of single crystalline silicon solar cells, Energy Convers. Manage. 46 (2005) 1485–1494.
[9] A. Jain, A. Kapoor, A new approach to study organic solar cell using Lambert W-function, Sol. Energy Mater. Sol. Cells 86 (2005) 197–205.
[10] M. Murayama, T. Mori, Equivalent circuit analysis of dye-sensitized solar cell by using one-diode model: effect of carboxylic acid treatment of TiO_2 electrode, Jpn. J. Appl. Phys., Part 1 45 (2006) 542–545.
[11] A. Ortiz-Conde, F.J. Garcia Sanchez, J. Muci, New methods to extract model parameters of solar cells from the explicit analytic solutions of their illuminated *I–V* characteristics, Sol. Energy Mater. Sol. Cells 90 (2006) 352–361.
[12] K.I. Ishibashi, Y. Kimura, M. Niwano, An extensively valid and stable method for derivation of all parameters of a solar cell from a single current–voltage characteristics, J. Appl. Phys. 103 (2008) 094507.
[13] M. Chegaar, N. Nehaoua, A. Bouhemadou, Organic and inorganic solar cells parameters evaluation from single *I–V* plot, Energy Convers. Manage. 49 (2008) 1376–1379.
[14] P. Mialhe, A. Khoury, J.P. Charles, Device-related phenomena a review of techniques to determine the series resistance of solar cells, Phys. Status Solidi A 83 (1984) 403–409.
[15] G. Li, et al., in: Exhibition in Solar Power International Conference 2009, Anaheim, California, October 27–29, 2009.
[16] F.C. Krebs, S.A. Gevorgyan, J. Alstrup, A roll-to-roll process to flexible polymer solar cells, manufacture and operational stability studies: models studies, J. Mater. Chem. 19 (2009) 5442–5451.
[17] F.C. Krebs, Fabrication and processing of polymer solar cells: a review of printing and coating techniques, Sol. Energy Mater. Sol. Cells 93 (2009) 394–412.
[18] G. Li, Y. Yao, H. Yang, V. Shrotriya, G. Yang, Y. Yang, Solvent annealing effect in polymer solar cells based on (Poly3 -hexylthiophene) and methanofullerenes, Adv. Funct. Mater. 17 (2007) 1636–1644.
[19] V.I. Arkhipov, P. Heremans, E.V. Emelianova, G.J. Adriaenssens, J. Bassler, Weak-field carrier hopping in disordered organic semiconductors: the effects of deep traps and partly filled density-of-states distribution, J. Phys. Condens. Matter. 14 (2002) 9899–9911.